Uphill Electron Transfer in the Tetraheme Cytochrome Subunit of the *Rhodopseudomonas viridis* Photosynthetic Reaction Center: Evidence from Site-Directed Mutagenesis[†]

I-Peng Chen,[‡,§] Paul Mathis,[||] Juergen Koepke,[‡] and Hartmut Michel*[,‡]

Max-Planck-Institut für Biophysik, Heinrich-Hoffmann-Strasse 7, D-60528 Frankfurt am Main, Germany, Section de Bioénergétique (CNRS, URA 2096), Bat. 532, CEA/Saclay, 91191 Gif-sur-Yvette, France

Received October 20, 1999; Revised Manuscript Received January 19, 2000

ABSTRACT: The cytochrome (cyt) subunit of the photosynthetic reaction center from *Rhodopseudomonas viridis* contains four heme groups in a linear arrangement in the spatial order heme1, heme2, heme4, and heme3. Heme3 is the direct electron donor to the photooxidized primary electron donor (special pair, P^+). This heme has the highest redox potential (E_m) among the hemes in the cyt subunit. The E_m of heme3 has been specifically lowered by site-directed mutagenesis in which the Arg residue at the position of 264 of the cyt was replaced by Lys. The mutation decreases the E_m of heme3 from +380 to +270 mV, i.e., below that of heme2 (+320 mV). In addition, a blue shift of the α-band was found to accompany the mutation. The assignment of the lowered E_m and the shifted α-band to heme3 was confirmed by spectroscopic measurements on RC crystals. The structure of the mutant RC has been determined by X-ray crystallography. No remarkable differences were found in the structure apart from the mutated residue itself. The velocity of the electron transfer (ET) from the tetraheme cyt to P^+ was measured under several redox conditions by following the rereduction of P^+ at 1283 nm after a laser flash. Heme3 donates an electron to P^+ with $t_{1/2} = 105$ ns, i.e., faster than in the wild-type reaction center ($t_{1/2} = 190$ ns), as expected from the larger driving force. The main feature is that a phase with $t_{1/2} \approx 2$ μs dominates when heme3 is oxidized but heme2 is reduced. We conclude that the ET from heme2 to heme3 has a $t_{1/2}$ of ∼2 μs, i.e., the same as in the WT, despite the fact that the reaction is endergonic by 50 meV instead of exergonic by 60 meV. We propose that the reaction kinetics is limited by the very uphill ET from heme2 to heme4, the $\Delta G°$ of which is about the same (+230 meV) in both cases. The interpretation is further supported by measurements of the activation energy (216 meV in the wild-type, 236 meV in the mutant) and by approximate calculations of ET rates. Altogether these results demonstrate that the ET from heme2 to heme3 is stepwise, starting with a first very endergonic step from heme2 to heme4.

Rhodopseudomonas (*Rps.*)[1] *viridis* is an anoxygenic purple non-sulfur photosynthetic bacterium. Like higher plants, algae, cyanobacteria, and many other bacteria, *Rps. viridis* performs photosynthesis in which light is converted into chemical energy. The energy conversion is mediated by a protein−pigment complex, called the photosynthetic reaction center (RC). Whereas higher plants, algae, and cyanobacteria utilize two types of RCs (photosystems I and II), anoxygenic photosynthetic bacteria possess only one of either type of RCs. The type-II bacterial RCs are membrane protein complexes containing L, M, and H subunits which are common to all RCs from purple bacteria. In many species such as in *Rps. viridis*, there is a fourth subunit, the cytochrome (cyt) *c* subunit, which is the electron donor for the photooxidized bacteriochlorophyll *b* dimer (P^+, so-called special pair) [for a review see Nitschke and Dracheva (*1*)]. The electron from P is transferred via the monomeric bacteriochlorophyll *b* and the bacteriopheophytin *b* on the "active-branch" to a menaquinone-9 (Q_A) molecule with a half-time of 200 ps (*2*, *3*). While the menaquinone-9 can only accept one electron, the second electron acceptor, a ubiquinone-9 (Q_B), is a two-electron carrier. After receiving two electrons and two protons, the doubly reduced ubiquinone-9, which has a lower affinity to the RC, diffuses out of the RC. The reducing equivalents on the reduced Q_B are delivered to the cyt bc_1 complex and from there to the periplasmic space in the form of a reduced cyt c_2, which subsequently donates an electron to the oxidized cyt bound to the RC and closes the light induced cyclic electron transfer (ET) process (*4*−*7*).

The cyt subunit of the *Rps. viridis* RC covalently binds four hemes, two of them are high-potential, and two low-potential. They are arranged in a linear manner roughly

[†] This work was financially supported by the Fonds der Chemischen Industrie and the Max-Planck-Gesellschaft.

* To whom correspondence should be addressed. E-mail: michel@mpibp-frankfurt.mpg.de. Phone: (+49) 69 96769401. Fax: (+49) 69 96769423.

[‡] Max-Planck-Institut für Biophysik.

[§] Current address: Institute of plant genetics and crop plant research Gatersleben, D-06466 Gatersleben, Germany.

[||] Section de Bioénergétique.

[1] Abbreviations: cyt, cytochrome; ET, electron transfer; Q_A, menaquinone-9; Mops, 4-morpholinopropanesulfonic acid; LDAO, *N*,*N*-dimethyldodecylamine-*N*-oxide; PMSF, phenylmethylsulfonyl fluoride; RC, reaction center; E_h, redox potential of the buffer; E_m, midpoint redox potential; *Rb.*, *Rhodobacter*; *Rps.*, *Rhodopseudomonas*; RMS, root-mean-square; P, special pair; Q_B, ubiquinone-9; WT, wild-type.

10.1021/bi992443p CCC: $19.00
Published on Web 03/10/2000

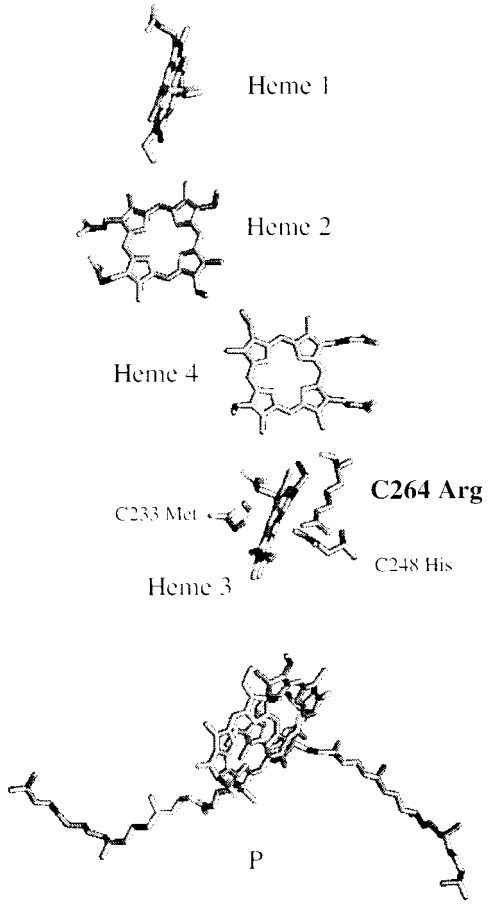

FIGURE 1: Arrangement of the heme groups in the cytochrome subunit of the WT *Rps. viridis* RC. The position of the C264 Arg residue relative to heme3 and the axial ligands of heme3 are also shown. The photoexcitable special pair situated in the transmembrane region below the heme3 is indicated as P. The hemes are numbered according to their appearance in the protein sequence.

perpendicular to the membrane with a spatial order from the periplasm towards the membrane as follows: heme1 (*c*-554, $E_m = -60$ mV), heme2 (*c*-556, $E_m = +320$ mV), heme4 (*c*-551, $E_m = +20$ mV), and heme3 (*c*-559, $E_m = +380$ mV) [Figure 1 (*8*−*10*)]. Heme3 is the closest heme to P and has the highest potential among the hemes. It transfers an electron to P^+ with a $t_{1/2}$ of 100−200 ns in solubilized RCs. The ET rate and the pathway are dependent on the redox state of the hemes and on the temperature (*11*, *12*). Consistent kinetic data have also been obtained with chromatophores and whole cells (*13*, *14*).

The RC from *Rps. viridis* has been crystallized and is the first membrane protein complex for which the structure has been determined at near atomic level, with a resolution of 2.3 Å (*15*, *16*). On the basis of the structural information and on theoretical studies (*17*), some amino acids have been proposed to have a significant influence on the redox potential. In particular, arginine C264 (the 264th residue of the mature cyt subunit), which is situated in the immediate vicinity of heme3 (Figure 1), is supposed to contribute by its positive charge to the high redox potential of heme3.

It has been well established that heme3 is the direct electron donor to P^+ when only high-potential hemes are reduced (*11*, *12*, *18*). The oxidized heme3 is rereduced by the other high-potential heme (heme2) when the latter is also prereduced. Heme4, which is the higher potential heme among the low-potential ones, has been detected to take part in the electron donation to P^+ under conditions where it is reduced (*11*, *12*). However, in view of the long distance (>23 Å) between heme4 and P^+, an ET rate obtained in a submicrosecond range ($t_{1/2} = 115$ ns) seems not to be conceivable for a direct ET. Straight evidence for the function of heme1 (the lowest-potential heme) is still not available. However, a role as an electron acceptor for the soluble electron donor (cyt c_2) has been suggested from kinetic and modeling studies (*19*). Further, this idea has been enforced recently by studies in mutant *Rubrivivax gelatinosus* RCs with mutations near the heme1 pocket (*20*). On the basis of a kinetic study of electron donation from cyt c_2 to *Rps. viridis* RC (*21*), it was proposed that, after docking, ET from cyt c_2 to heme2 (cyt *c*-556) takes place in two steps: a first very endergonic (rate limiting, $t_{1/2} = 60$ μs) ET to heme1 (*c*-554), followed by a very fast ($t_{1/2}$ below 1 ns) ET to heme2.

The cyt subunit of *Rps. viridis* RC, although it has been extensively studied by spectroscopy (*12*, *14*, *22*−*26*), is still mysterious in some aspects including (1) the precise function of the four hemes, especially the role of the two low-potential hemes, in ET, (2) the meaning of the alternative arrangement of the hemes with the potential sequence low-high-low-high, and (3) the detailed pathway of the ET. In addition, the interheme ET from heme2 to heme3 has been found to have a half-time of about 2 μs (*8*, *12*, *14*, *18*, *26*) despite the long edge-to-edge distance of 21.4 Å. Heme4, which is situated between heme2 and heme3, has not been shown to participate in this ET. For the participation of heme4, the electron would have to go through a thermodynamically unfavorable (or uphill) step, since the E_m of hemes 2 and 4 are +320 and +20 mV, respectively. The question is addressed in the present work.

We describe the construction and characterization of a mutant RC (C264RK) in which Arg C264 has been replaced by Lys. In the mutant RC, the midpoint potential of the highest potential heme (heme3) has been selectively lowered, so that it becomes lower than that of heme2. Kinetics of the ET from heme2 and heme3 to the special pair have been studied. The kinetic data support the active role of heme4 in the reduction of heme3, and an uphill ET step from heme2 to heme4 is proposed to be the rate-limiting step with a $t_{1/2}$ of about 2 μs.

MATERIALS AND METHODS

Bacterial Strains and Growth Conditions. The *Rps. viridis pufC* deletion strain, in which the coding region for the *Rps. viridis pufC* gene was replaced by a kanamycin cassette (*27*), was made available by Prof. D. Oesterhelt (unpublished). This strain was grown under microaerophilic conditions (*28*). Recombinant *Rps. viridis* cells were grown under phototrophic conditions in sodium succinate medium (*29*). *Escherichia coli* strain XL 1-Blue was used for cloning purposes and was grown aerobically at 37 °C in Luria-Bertani medium [10 g of Bacto Tryptone, 5 g of yeast extract, and 10 g of NaCl/L (pH 7.2)]. Appropriate antibiotics [ampicillin (100 μg/mL), kanamycin (20 μg/mL), and/or tetracycline (12.5 μg/mL)] at the indicated concentrations supplemented the growth media.

DNA Manipulations and Sequencing. DNA treatments and transformation of *E. coli* with plasmids were performed with

standard methods. For small-scale preparation of plasmid DNA from *Rps. viridis*, cells at late log-phase were collected from a 2 mL culture (Eppendorf microfuge 14 000 rpm, 5 min at room temperature). The cells were resuspended in 200 μL resuspension buffer [50 mM Tris/HCl (pH 7.5), 10 mM EDTA with 20 μg of RNase A and 0.5 mg of proteinase-K] and incubated at 37 °C for 10 min. The same volume (200 μL) of cell lysis buffer (0.2 M NaOH, 1% SDS) was added to the cell suspension and incubated for another 10 min. The cell lysate was neutralized with 200 μL of neutralization buffer [1.32 M potassium acetate (pH 4.8)]. A clear cell lysate was obtained by centrifugation (Eppendorf microfuge 14 000 rpm, 10 min at room temperature). The clear cell lysate was mixed with 1 mL of Wizard minipreps DNA purification resin and applied to a Wizard minicolumn (Promega). The DNA was washed and eluted as described by the manufacturer (Promega). The isolated plasmid-DNA could be subjected to restriction digestion analysis. DNA sequencing was performed using the T7 sequencing kit from Pharmacia Biotech. The Genetics Computer Group software package (GCG) was used for analysis of DNA and protein sequences (*30*).

Site-Directed Mutagenesis. Mutagenesis was carried out using the method of Kunkel (*31*). The sequence of the oligonucleotide synthesized on a model 392A-05 Applied Biosystems automated DNA synthesizer for the mutagenesis is as follows: 5′-GCC CCA CCA CG*C GAT CG*C **CTT** CTG CGG CGT GCT CTT-3′. The Arg to Lys mutation is shown as bold letters (**CTT**, complementary sequence) and silent mutations (italics) were introduced for screening mutant candidates. The presence of the desired mutation was confirmed by sequence analysis.

Electroporation of the Rps. viridis pufC Strain. The plasmid constructions for the WT and the mutated *pufC* gene were introduced into *Rps. viridis pufC* deletion strain via electroporation. Competent cells were prepared according to the suggestions of the manufacturer of the electroporation apparatus (Bio-Rad). A total of 40 μL of competent cells (10^7-10^9 cells/mL) was transformed with 1 ng to 1 μg plasmid DNA using a 0.2-cm electroporation cuvette with a field strength of 12.5 kV/cm [at 25 μF, 2.5 kV and at 600 Ω (*27*)]. Using such conditions, a time constant between 10 and 14 ms was usually obtained. After electroporation, the cells were incubated in N-medium (2 mL) containing 20 mM glucose in a 2 mL Eppendorf tube in the dark overnight and transformants were selected on solid medium containing appropriate antibiotics.

Purification of Recombinant RCs. Rps. viridis cells were collected from liquid culture by centrifugation (5000*g*, 10 min) and were resuspended in TNE buffer [10 mM Tris-HCl (pH 8), 100 mM NaCl, 1 mM EDTA] with 1 mM phenylmethanesulfonyl fluoride (PMSF) to a concentration of 175 mg of cells (wet weight)/mL buffer. The cells were broken by sonication (Branson sonifier 250, resonator with 12.6-mm tip, output 10, duty cycle 50%) for 45 min in an ice−water bath. The intact cells were collected by centrifugation (20000*g*, 20 min at 4 °C) and sonified as before and centrifuged again. Both fractions of supernatant were pooled and centrifuged (150000*g*, 90 min at 4 °C) to obtain the crude membranes (pellet). The crude membranes can be stored at −70 °C or be used immediately for solubilization. For solubilization, the crude membranes were resuspended in TNE buffer (with 1 mM PMSF) to $OD_{1010} = 50$. From this step on, all procedures were performed in the dark at 4 °C, unless otherwise stated. To solubilize the RCs, 30% (w/v) LDAO (*N*,*N*-dimethyldodecylamine-*N*-oxide) was added slowly to the membrane suspension to a final concentration of 1%. After 30 min of stirring, the solution was centrifuged (150000*g*, 90 min) and the supernatant was collected. The pellet was resuspended in TNE buffer (with 1 mM PMSF) to $OD_{1010} = 100$, stirred with 1.8% LDAO, and centrifuged as before. These two portions of supernatant (containing the solubilized RCs) were pooled and a spectrum was recorded from 400 to 1100 nm. The solubilized RCs were subsequently subjected to chromatography. Due to the fusion of a His_6-tag (*32*, *33*) to the C-terminus of the cyt *c* subunit of the recombinant RCs, the RCs could be purified via a Ni-NTA agarose column (Qiagen) followed by a gel-filtration chromatography step [Fractogel TSK HW-55 (S) column (Merck)]. For this purpose, the supernatant of the solubilization was diluted with 4 vol of TNL buffer [10 mM Tris-HCl (pH 8), and 100 mM NaCl, 0.1% LDAO] and applied onto a Ni-NTA agarose column (dimensions 7 cm × 1.5 cm). The column was washed with TNL buffer containing 10 mM imidazole, and bound RCs were eluted with 50 mM imidazole (in TNL buffer). Partially purified RCs (with the ratio of $A_{280}/A_{830} \leq 3$) were collected, concentrated (to 5−10 mL), and applied onto a gel filtration column [Fractogel TSK HW-55 (S) with dimensions of 90 cm × 2.5 cm]. Phosphate buffer [20 mM NaH_2PO_4 (pH 6.0), 0.12% LDAO, 1 mM sodium azide] was used for the equilibration of the column and the elution of RCs. Fractions with a ratio of $A_{280}/A_{830} \leq 2.1$ were collected for crystallization and kinetic and spectroscopic studies. The concentration of RCs was determined spectroscopically using $\epsilon = 280000\ M^{-1}\ cm^{-1}$ at 830 nm (*34*).

Redox Titrations. The redox titration of the high-potential and low-potential hemes of the C264RK RC in solution was carried out in a 1 cm × 1 cm cell aerobically and anaerobically, respectively. Difference spectra at various E_h values versus an appropriate reference were recorded with a Perkin-Elmer UV/VIS spectrometer Lambda 40. The redox potential was measured with an Ag/AgCl electrode (Microelectrodes Inc.) connected to a Mettler delta 345 voltmeter. For the high-potential titration, the sample cell contained 2 μM RCs in 25 mM 4-morpholinopropanesulfonic acid [Mops (pH 7.0)], 0.1 M KCl, and 0.1% Triton X-100 at 25 °C. Redox mediators: 200 μM 3,6-diamino-durol (DAD) and 50 μM 1,4-benzoquinone were added into the sample cell. For the titration, the sample was first oxidized with potassium ferricyanide and then slowly reduced by the addition of ascorbate and subsequently back-titrated with potassium ferricyanide. For the low-potential titration, the sample cell contained 2 μM RCs in 25 mM Tris-HCl (pH 8), 100 mM KCl, 0.1% Triton X-100 at 25 °C. Redox mediators (each 50 μM): 1,2-naphthoquinone-4-sulfonate, 4-amino-4-methoxydiphenylamine (HCl salt), anthraquinone, anthraquinone 2,6-disulfonate (Na salt), anthraquinone 2-sulfonate (Na salt). For the titration, the sample was slowly reduced by the addition of sodium dithionite and then back-titrated with potassium ferricyanide.

Redox titration of the high-potential hemes was also performed with RC crystals to determine the midpoint redox potential of each heme groups. The titration was performed

according to Fritzsch et al. (*9*). Stabilization of the redox potentials was achieved by addition of four redox mediators (each 50 μM): *p*-diphenylamine sulfonic acid (Na salt), 1,4-benzoquinone, 1,2-naphthoquinone-4-sulfonic acid (Na salt), and 4-amino-4-methoxy diphenylamine (HCl salt). The redox potentials were adjusted by the addition of ferricyanide (for the oxidation) and by ascorbate (for the reduction).

Kinetics of the ET from the Cytochrome to the Special Pair. LDAO-solubilized RCs [2 μM in 40 mM Tris-HCl (pH 8.0), 0.05% LDAO] were poised at appropriate redox states in the presence of 100 μM of redox mediators: DAD and vitamin K_3. The redox potential was adjusted by the addition of potassium ferricyanide, potassium ferri/ferrocyanide or ascorbate. P^+ formation and P^+ rereduction were recorded at 1283 nm (*12*). The cuvette was excited by short saturating flashes (10 ns, 694 nm) provided by a ruby laser. The time resolution was 40 ns. For the low-temperature measurements, glycerol was added to the samples at a final concentration of 60% (v/v). The cuvette, with optical paths of 10 mm for the measuring light and 4 mm for excitation, was inserted into a cryostat cooled with liquid nitrogen. Recordings resulting from four flashes separated by 1 min were averaged. The kinetic traces obtained from the measurements were treated as sums of several exponential components to find $t_{1/2}$ values (or rates: $k = 0.693 t_{1/2}^{-1}$) and amplitudes. Exponential analyses were performed by the Marquardt method with a software devised by Dr. P. Sétif. Due to instability of the laser diode used as a source of measuring light, signals slower than 200 μs have very unprecise kinetics.

Crystallization and Structure Determination. Purified RC was crystallized under the same conditions as for the WT RC (*35*). Crystals isomorphous to the WT RC crystals were obtained after 1 week. Data acquisition was performed at a temperature of 4 °C (at the crystal). Diffraction data were collected using monochromatic synchrotron radiation with a wavelength of 0.91 Å at the EMBL X11 beamline at HASYLAB, Hamburg (Table 1). Rotational photographs with an oscillation range of 0.4° were taken on a MAR Research image plate detector from crystals oriented with their crystallographic *c*-axis about parallel to the φ-axis of the diffractometer. The measured data set has a resolution of 2.46 Å with a completeness of 81% for significant observations [$F > 2\sigma(F)$]. The images were processed with the program DENZO (*36*). The crystal structure of the mutant RC was determined using the most recent WT structure [2PRC (*37*)]. Crystallographic refinement was performed using repeated cycles of simulated annealing, conventional positional refinement, isotropic individual *B* factor refinement with the program X-PLOR [version 3.1 (*38*)]. Manual inspection and refitting were done with the molecular graphics program O (*39*). Table 1 contains a summary of refinement statistics.

Table 1: Data Collection and Structure Refinement of the *Rps. viridis* C264RK RC

Data	
high-resolution limit (Å)	2.46
no. of measured reflections	183 066
no. of unique reflections (multiplicity)	89 461 (2.18)
completeness (%) (at high resolution)	81.0 (86.1)
R_{sym} (%)[a]	7.3
$I/\sigma(I)$ (2.48−2.46 Å)	6.27
Refinement	
R_{free} (%)[b] (10.0−2.46 Å)	22.6
R factor (%)[c] (10.0−2.46 Å)	18.7
maximum coordinate error (Å)[d]	0.3
no. of nonhydrogen atoms in the model	11 496
average *B* factors (Å^2)	
main chain	22.9
side chain	23.7
cofactors	29.0
water molecules	32.7
rms deviations from ideal values	
bond lengths (Å)	0.017
bond angles (deg)	1.71
dihedral angles (deg)	23.8
improper torsion angles (deg)	2.56

[a] $R_{sym} = \sum_{hkl}\sum_i |I_i - \langle I\rangle| / \sum \langle I\rangle$, I_i is the intensity of the *i*th measurement of reflection *hkl* and $\langle I\rangle$ is the average intensity of a reflection. [b] R_{free} is calculated from 5% of the measured unique data that were not used during refinement. [c] $R = \sum |F_o - kF_c| / \sum |F_o|$, where F_o and F_c are the observed and calculated structure amplitudes, respectively, and *k* is a scaling factor. [d] Estimate of the mean coordinate error from a Luzzati plot (*50*).

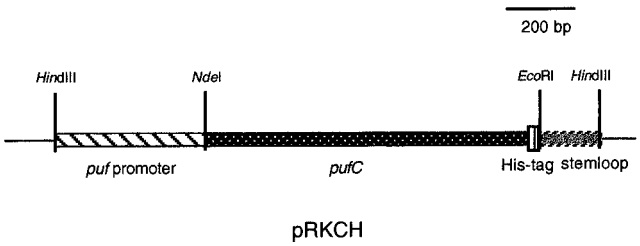

FIGURE 2: Plasmid pRKCH for the expression of the *pufC* gene in the *Rps. viridis pufC* deletion strain. It contains three parts: the promoter region of the *Rps. viridis puf* operon, the complete *pufC* gene with a His_6-tag extension on the C-terminus, and a stem loop of the *puf* operon.

RESULTS

Construction of Plasmid pRKCH, Site-Directed Mutagenesis and Purification of the RCs. For the expression of mutant *Rps. viridis* RCs in the *pufC* deletion strain (D. Oesterhelt, unpublished) a plasmid pRKCH has been constructed in this work (Figure 2). The insert of this plasmid contains three parts: the promoter region of the *Rps. viridis puf* operon [bp nos. 545−954 of the *Rps. viridis puf* promoter region, sequence from GenBank with the accession number M55261 (*40*)], the complete cyt subunit, gene *pufC* (*41*), and a piece of DNA coding for a stem loop of the *puf* operon [bp nos. 1395−1506 of M55261]. To facilitate the purification of RCs, DNA coding for a His_6-tag was fused to the C-terminus of the *pufC* gene. All these DNA parts were amplified by PCR, and their sequences were confirmed. In the mutant RC, the Arg at position 264 in the cyt subunit (C264) was thus substituted by a Lys residue (C264RK). Both the WT and mutant plasmid constructions could restore the photosynthetic competence of the *Rps. viridis pufC* deletion strain and the RCs could be isolated. Due to the attachment of the His_6-tag to the C-terminus of cyt subunit, the purification of the recombinant RCs has been greatly simplified and the tag did not induce any changes in the redox properties and the absorption spectrum in the range of 400−1100 nm of the RCs (not shown).

Structure of the C264RK RC. The C264RK RCs were crystallized under the same conditions as the WT RCs, and crystals isomorphous to the WT RC crystals ($P4_32_12$, tetragonal) with cell dimensions of $a = b = 223.5$ Å and *c*

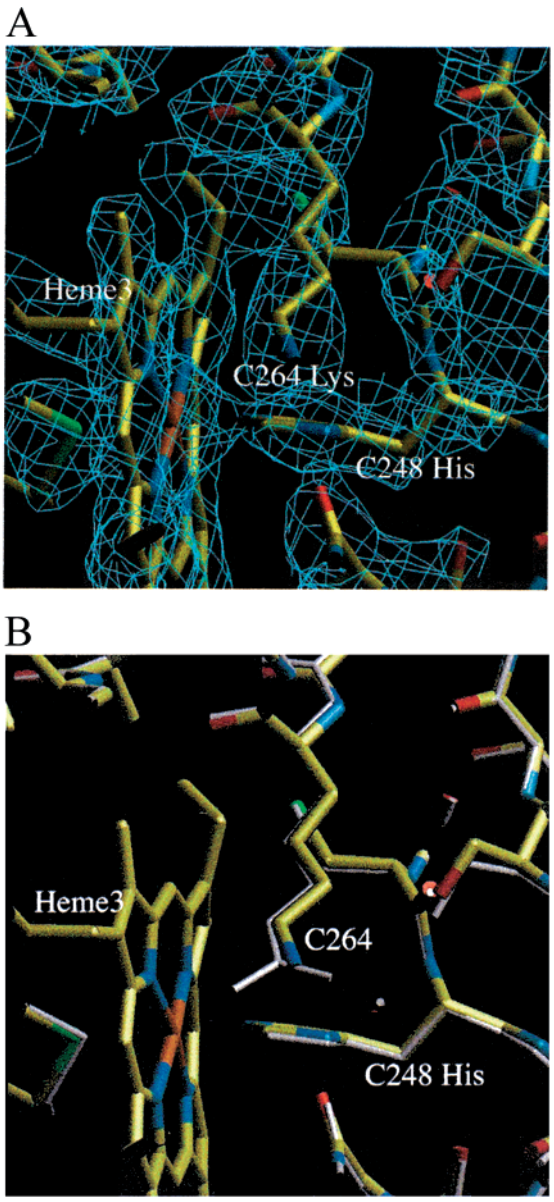

FIGURE 3: Structure of the C264RK RC at the C264 Lys residue and in its surroundings. (A) $2F_o - F_c$ electron density map for the C264 Lys residue at a contouring level of 2σ. (B) Comparison of the structure of the C264RK RC (thick line) with that of the WT (thin line) at the mutation site (the residue C264).

= 113.7 Å were obtained after 1 week. A single crystal was used for the collection of a data set with a resolution of 2.46 Å. Data collection and the refinement statistics are listed in Table 1. Apart from the site of the amino acid change, the overall structure of the C264RK RC does not significantly deviate from that of the WT (RMS deviation = 0.12 Å). The distances among hemes and between them and the special pair remain essentially unchanged. Even in the immediate vicinity of the C264 Lys residue, the mutation does not induce remarkable structural changes. The electron density of C264 Lys and its surroundings is shown in Figure 3A and a comparison of the mutant structure with that of WT around C264 is presented in Figure 3B. No extra electron density for the His_6-tag at the C-terminus of the cyt subunit was detected. This implicates that in the mutant RC the C-terminus of the cyt is also disordered as already seen in the WT RC (*16*).

Spectral Characterization and Redox Properties of the Hemes of the C264RK RC. The absorption spectrum in the range of 400−1100 nm of the solubilized C264RK RCs was compared with that of the WT. The only difference was found in the α-band region (550−560 nm) of the heme groups. Therefore, absorption spectra in the α-band region of the C264RK RCs were recorded under different redox conditions at 25 °C and were compared with those of the WT RCs. The difference spectrum (mutant RC minus WT) measured at +300 mV (at which the WT heme3 is completely reduced and heme2 is also mostly reduced) shows a negative peak at 559 nm which is the characteristic position of the α-band of heme3 in the WT RC (Figure 4A). The result suggests the absence of the reduced form of heme3 in the mutant RC under such redox conditions. In the mutant RC, the two high-potential hemes could be reduced completely only at a lower redox potential (+210 mV, not shown) than in the WT RC (+250 mV, not shown). At +190 mV, where both high-potential hemes (heme2 and heme3) of the WT and mutant RCs are reduced, the difference spectra (two hemes reduced minus oxidized) show a blue shift of the α-band for C264RK RCs [from 557.5 nm in the WT to 554 nm in the mutant (Figure 4B)]. For the redox titration of the high-potential hemes of the mutant RC (see below), the absorption changes upon different redox conditions was therefore monitored at 554 nm instead of 557.5 nm, which was chosen for the WT. The difference spectrum (mutant minus WT) in a state with two hemes reduced shows a positive peak at 552 nm and a negative peak at 559 nm with the same amplitude (Figure 4C). The results imply that the replacement of arginine by lysine has altered the spectrum of reduced heme3 and led to a blue shift of 7 nm. Consistently, a characteristic shoulder at 552 nm has also been previously reported for the reduced heme3 (*8*). The tentative assignment of this 552 nm α-band in the mutant to the modified heme3 was further confirmed by the spectroscopic studies on RC crystals. In contrast to the differences in the reduced state, the mutation did not affect the oxidized spectrum of the cyt (not shown).

Due to the complexity of the spectra of the multiheme cyt of the *Rps. viridis* RC, the assignment of individual hemes with respect to their α-band absorption, spatial arrangement, and redox properties was difficult. However, spectroscopic studies with ordered RCs (e.g., with crystals) have provided well-resolved and unambiguous data (*9*). In the *Rps. viridis* RC crystal, the hemes can be roughly divided into two classes according to the orientation of their heme planes. The planes of heme1 and heme3 are essentially parallel to the *z*-axis of the crystal, the other two hemes (heme2 and heme4) are rather perpendicular to the *z*-axis. These two classes of hemes can be easily distinguished from each other by their absorption of polarized light (*9*). To investigate the origin of the α-band at 552 nm (see the difference spectrum in Figure 4C), spectroscopic studies on a crystal of C264RK RC with polarized light were performed. Clearly, a peak at 552 nm was obtained from the difference spectrum [two hemes reduced (+220 mV) minus oxidized (+470 mV), Figure 4D], when the polarized light was parallel to the *z*-axis. Altogether, the results demonstrate that the mutation changes the spectral characteristics at heme3 and lowers its redox midpoint potential.

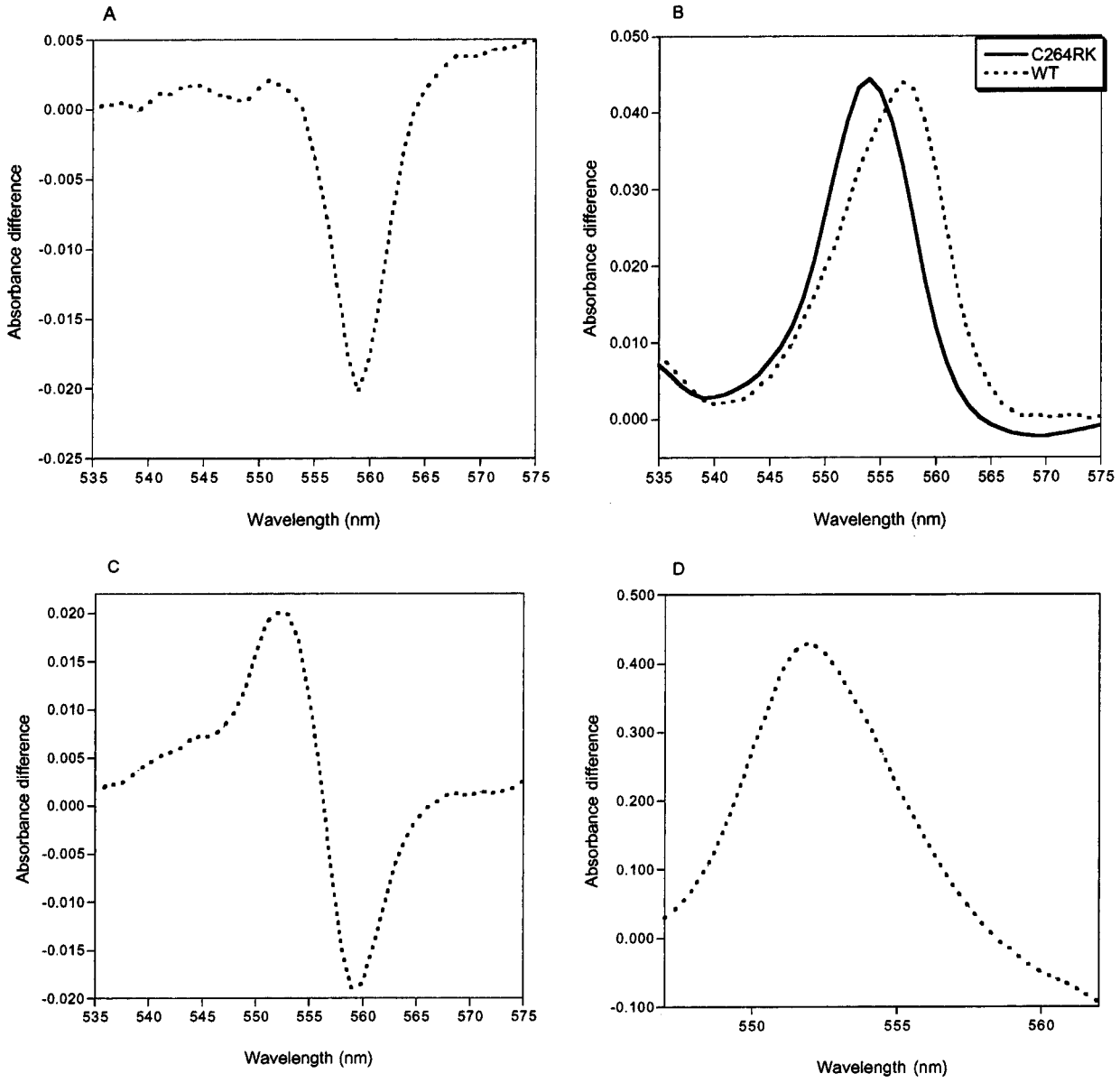

FIGURE 4: Difference spectra of the high potential hemes of the cyt subunit of the WT and the mutant (C264RK) RCs under different redox conditions. (A) Difference spectrum (mutant minus WT) of the α-band region at +300 mV. (B) Difference spectrum [both high potential hemes reduced (+190 mV) minus oxidized (+440 mV)] of the WT RC (dashed line) and the C264RK RC (solid line). (C) Difference spectrum (mutant minus WT) of the α-band region at +190 mV. (D) Difference spectrum [reduced (at +220 mV) minus oxidized (at +470 mV)] of the α-band region of the heme3 in the mutant RC measured with the RC crystal. The polarized light was parallel to the *z*-axis of the crystal. LDAO-solubilized RCs were used for measurements in panels A, B, and C.

To quantify the decrease of the midpoint potential of the modified heme3, the E_m values of the high-potential hemes have been determined by redox titration. The titration was first performed on solubilized RCs by determining the absorption changes at 554 nm as a function of the redox potential. The data of the titration could be fit well with the Nernst equation for two one-electron components (the line drawn in Figure 5). The midpoint potentials of the two high-potential hemes deduced from the fit are +320 mV (ranging between +300 and +340 mV in several measurements) and +270 mV (between +260 and +280 mV). These were tentatively assigned to heme2 (the published data for heme2 of the WT RC range from +290 to +320 mV) and to the modified heme3, respectively. This assignment was latter confirmed by a redox titration with the RC crystal, which gave the same results (not shown). E_ms of the low-potential hemes were examined with solubilized RCs and no effect of the mutation was observed: E_ms of about +15 and −60 mV were obtained.

Kinetics of the ET from the Tetraheme Cytochrome to the Special Pair. The ET from the tetraheme cyt to the special pair was studied by measuring the rereduction of flash-induced P^+ in isolated RCs under four different redox conditions at room temperature. Figure 6 shows typical kinetic traces of flash-induced absorption changes in the near-infrared P^+ absorption band (1283 nm) for the C264RK RC. The kinetic traces were analyzed with three to five exponential components as shown in Table 2. At a redox potential of +410 mV, where nearly all of the hemes of the C264RK RCs were in the oxidized state (a few percent of heme2 might be reduced), most of P^+ decayed in hundreds of milliseconds, a reaction attributed to recombination of the reduced secondary quinone Q_B^- with P^+. No sub-microsecond phase was detectable. A small phase with $t_{1/2}$ = 2.2 μs (3.9%) was

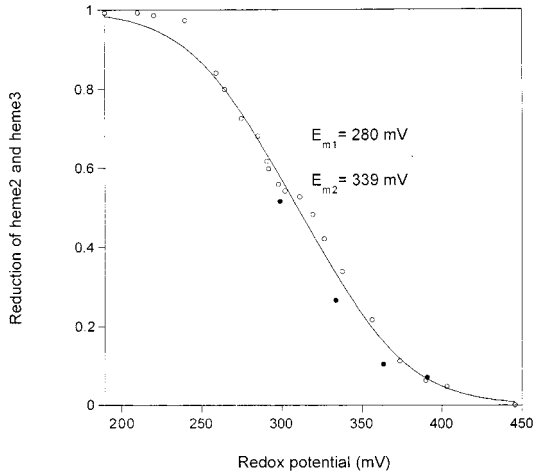

FIGURE 5: Redox titration of the high-potential hemes of the cyt subunit of the mutant *Rps. viridis* RC (C264RK). The sample cell contained 2 μM RCs in 25 mM 4-morpholinepropanesulfonic acid (Mops, pH 7.0), 0.1 M KCl, and 0.1% Triton X-100 at 25 °C. Redox mediators: 200 μM 3,6-diamino durol, 50 μM 1,4-benzoquinone, and 2 mM potassium ferricyanide. For the titration, the sample was slowly reduced by the addition of ascorbate (○) and back-titrated with potassium ferricyanide (●). At each point the absorption of the α-band (554 nm) of the hemes relative to the absorption at 567 nm was recorded. The data were fitted with the Nernst equation for two one-electron components (solid line).

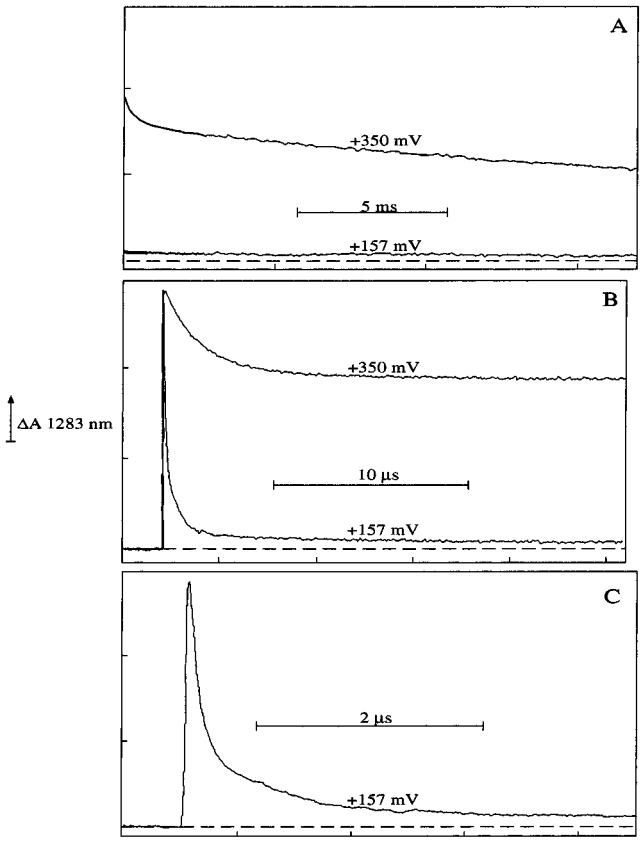

FIGURE 6: Time-resolved flash-induced absorption changes at 1283 nm of C264RK RC poised at +157 mV or +350 mV at 293 K. The curves are the result of a single laser flash. They are shown on three time scales (the +350 mV curve was omitted at the fastest scale because its kinetics appears fairly well on the 10 μs scale).

consistently observed, which we attribute to RCs having heme2 reduced. Two middle phases with $t_{1/2}$ around 200 and 700 μs (7−10% altogether) could be due, at least in part, to recombination of the reduced primary quinone Q_A^- with P^+. At a redox potential of +350 mV where about 30% of heme2 and practically no heme3 is reduced before the flash, there was again no sub-microsecond phase, but the fast phase had a total weight of ∼35%. It could be decomposed into two components of 2.2 and 3.9 μs, with respective weights of about 3:1. Slower phases had $t_{1/2}$ of about 250 μs, 1.4 ms, and 69 ms; they were probably due to backreaction from Q_A^- and Q_B^-. The fast phases (2.2 and 3.9 μs) were attributed to the reduction of P^+ by heme2, because under these redox conditions, heme2 was the only reduced heme in the tetraheme cyt. The mechanism of this reaction will be discussed below. Preliminary titrations were performed by additions of potassium ferro- and ferricyanide. They showed that the slow phases of P^+ rereduction globally titrate with $E_m \approx 340$ mV, simultaneously with the appearance of the 2.2 and 3.9 μs. A series of measurements were also performed at $E_h = +157$ mV, a potential at which both high-potential hemes (heme2 and heme3) were fully reduced. A fit of the data required four exponentials with $t_{1/2}$ of 105 ns (75.8%), 856 ns (20.4%), 11.7 μs (2.4%), and more than 200 μs (1.4%). The phases with $t_{1/2} = 2-4$ μs were absent; they clearly reappeared upon oxidation by progressive addition of ferricyanide. Experiments at +90 mV, where heme4 was partly reduced, showed a further acceleration of the very fast phase to 87 ns, the true $t_{1/2}$ probably being shorter due to the slow time response of the apparatus; the ∼900 ns phase was not present any longer, whereas a small 2.2 μs phase was present (but not always) and a phase with 11.2 μs was of higher amplitude. The latter component has been attributed to the triplet state ^3P which could be formed in RCs where Q_A is reduced (*12*). A slight reoxidation led to properties similar to those found at +157 mV (in particular the reappearance of the phase around 900 ns and a decrease of the 11 μs component). The effects of temperature on the kinetics have been studied at +350 mV in the temperature range 296−244 K. Two main features were observed. First, the fraction of P^+ that decays in a few microseconds decreases and is nearly zero at 240 K. At that temperature, P^+ decays entirely in a millisecond phase, i.e., by recombination with Q_A^- or Q_B^-. This behavior has already been studied in detail (*12*), but it remains unexplained. The second observation is a slowing of the microsecond reaction, as shown in Figure 7 in an Arrhenius plot. For that plot, we have not attempted to differentiate two phases in the microsecond decay because such a differentiation is not possible when the extent of these phases decreases. From the Arrhenius plot of Figure 7, we obtain an activation energy of 236 meV.

DISCUSSION

In this work, we show that the midpoint potential of heme3 of the cyt *c* bound to *Rps. viridis* RC is lowered from 380 to 270 mV by site-directed mutagenesis where the C264 Arg is replaced by Lys. In the mutant RC, its E_m is lower than that of heme2, changing the normal redox sequence in the tetraheme subunit. The mutation did not cause any significant structural modification apart from the residue C264 itself. Thus, the ET could be investigated in more detail, especially with respect to the influence of the driving force.

For mutagenesis, a suitable expression system including a host strain and an appropriate plasmid is required. For

Table 2: Half-Times and Relative Amplitudes of the Decay Phases of Flash-Induced Absorption Changes at 1283 nm in *Rps. viridis* C264RK RC Poised at Different Redox Potentials, at 293 K[a]

	kinetic phases						
redox state	phase I	phase II	phase III	phase IV	phase V	phase VI	slow phase
+410 mV very small fraction of reduced heme2			2.15 μs (3.9%)		195 μs (4.5%)	695 μs (4.2%)	(87.4%)
+350 mV only heme2 partially reduced			2.2 μs (26.2%) + 3.85 μs (8.7%)		248 μs (6.3%)	1.4 ms (7.3%)	(51.5%)
+157 mV heme2 and heme3 reduced	105 ns (75.8%)	856 ns (20.4%)		11.7 μs (2.4%)			(1.4%)
+90 mV heme4 also partially reduced	87 ns (70.3%)		2.2 μs (3.8%)	11.2 μs (23.7%)			(2.2%)

[a] Experimental curves were analyzed in exponential components according to the Marquardt method. The $t_{1/2}$ values are classified in different groups. The uncertainty on the kinetic values increases progressively above 200 μs because of fluctuation of the measuring light. For phases V and VI, the $t_{1/2}$ are within a factor of 2. The Slow phase is slower than 10 ms. Phase I, especially at +90 mV, is presumably lengthened by the instrument time-response of about 50 ns.

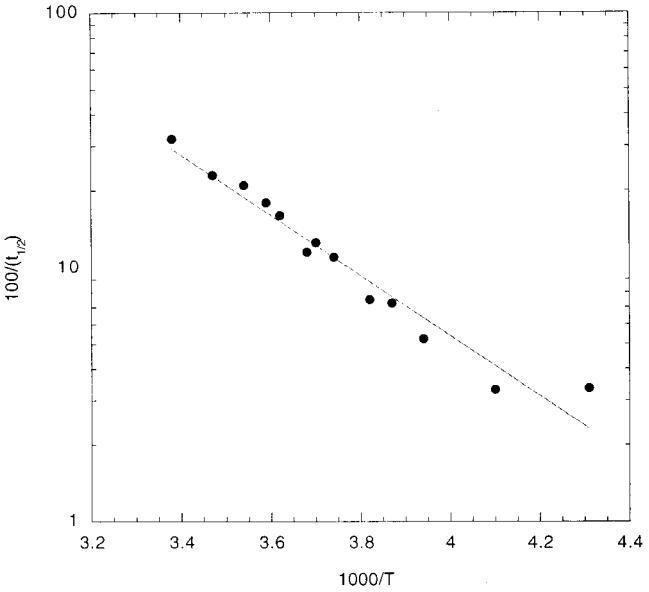

FIGURE 7: Arrhenius plot for the microsecond phase of P^+ reduction in mutant RC. In a cuvette with 60% glycerol (v/v), the redox potential was poised by addition of 5 mM potassium ferrocyanide, 0.5 mM potassium ferricyanide, 2.5 μM DAD, and vitamin K_3. The microsecond phase represents 75% of the total signal at 296 K and 21% at 244 K.

mutation in the cyt subunit of the *Rps. viridis* RC, a *Rps. viridis pufC* deletion strain was provided by D. Oesterhelt. A pRK404-based expression plasmid (pRKCH) comprising the *puf* promoter region, *pufC* gene (in the form of a replaceable cassette) and a piece of DNA-forming stem loop was constructed in this work. This plasmid has been shown to be functional in the *Rps. viridis pufC* deletion strain and RCs could be obtained. The *Rps. viridis pufC* gene is a part of the *Rps. viridis puf* operon, which contains genes encoding the light harvesting complex, and the L, M, and C subunits of the RC (*40*). Another pRK404-based plasmid (pRKML), which contains the whole *puf* operon has been used for expression of *Rps. viridis* RCs with modifications in the L and M subunits (*27*). The big size of the insert (8.8 kb) of that plasmid, however, made its handling very difficult. In contrast, the plasmid used here has an insert of only 1.6 kb and confers advantages for the mutagenesis due to its replaceable gene cassette. Furthermore, the fusion of a His_6-tag to the C-terminus of the cyt has greatly simplified and shortened the purification process without disturbing the structure and function of the RC.

One of the goals of this work was to explore and to verify the determinants for the redox midpoint of heme3 of the *Rps. viridis* RC and to modify it. The E_ms of the four hemes of the cyt subunit extend over ~400 mV. The differences in the E_ms of these hemes are the results of interactions of the heme cofactors with their surroundings and are strongly dependent on the nature of the hemes and the protein environment. In general, the axial ligands of the heme iron, the p*K* values of the heme propionates, and existence of charged residues which are in close contact with the heme are of great importance in determining the midpoint of a heme (*42*). In a theoretical work by Gunner and Honig (*17*), the effects of these factors on the E_ms of the hemes were studied, and results consistent with the experimental data were obtained. Among other determinants, an Arg residue at C264 has been highlighted as an important factor stabilizing the reduced form of heme3 with an electrostatic free energy of oxidation ($\Delta G°$) of 364 meV. In this work, we have experimentally confirmed the role of this residue through site-directed mutagenesis, since a drastic decrease of more than 100 mV in the E_m for heme3 was induced by substituting Arg C264 with a Lys. To exclude that the observed changes result from large structural differences, the structure of the mutant was determined by X-ray crystallography. The overall structure of the RC and even the local structure around the residue C264 did not show any significant difference to the WT RC (apart from the mutation itself, see Results). Thus the decrease in the E_m for heme3 in the mutant RC could be mostly attributed to the lower pK_a nature of Lys compared to that of the original residue (Arg) in the WT RC.

A blue shift in the α-band of heme3 by 7 nm was also observed in the C264RK RC. The blue shift indicates that the electronic structure of heme3 has been modified by the mutation. Actually, a well-defined shoulder at 552 nm has been reported for heme3 of the WT RC (*8*). This shoulder has been interpreted as a result of the asymmetry of the heme3 environment, e.g., a strain in the axial ligation. In the mutant, a shoulder at 559 nm for the α-band of heme3 could not be detected. The disappearance of the absorption at 559 nm which shifts to 552 nm presumably reflects a greater symmetry of the heme3 environment in the mutant.

For the discussion of the ET, we will focus on two redox states, at 157 and 350 mV, which representatively cover the

kinetics of interest. Since the WT and the mutant RC have the same structure, we will relate the kinetic differences to changes in redox potentials, assuming that the reorganization energies for the reactions are not changed and that the P/P^+ couple has the same E_m of 500 mV. At 157 mV, we can assume that both heme2 and heme3 in the C264RK RC are reduced before the flash. The situation is analogous to that studied by Ortega and Mathis (*12*) with the WT RC having two hemes reduced. A major phase of the P^+ reduction then took place with $t_{1/2} = 190$ ns, attributed to the ET from heme3 to P^+. Here for the mutant, the $t_{1/2}$ of the major phase is 105 ns. Since the distance between heme3 and P^+ is the same in both cases, we attribute the acceleration in the mutant RC to the larger driving force: 230 meV instead of 134 meV [in the WT we include an additional electrostatic energy of 14 meV due to the interaction between high-potential hemes, as calculated by Gunner and Honig (*17*); this energy is not added in the mutant RC, because heme3 has been titrated when heme2 was already reduced]. Interestingly, the $t_{1/2}$ of 105 ns obtained with $\Delta G° = -230$ meV compares well with that obtained for the same reaction when three hemes are reduced in the WT RC: $t_{1/2} = 110$ ns with a $\Delta G°$ estimated as -211 meV [120 meV due to the measured redox potentials of heme3 and P^+, plus interaction energies of 77 and 14 meV due to the additional reduction of heme4 and heme2, respectively, as discussed in Ortega and Mathis (*12*), on the basis of the calculations by Gunner and Honig (*17*)]. A quantitative treatment can be done with the empirical formula of Moser and Dutton (*43*):

$$\log k = 15 - (0.6\ \text{Å}^{-1})R - (3.1\ \text{eV}^{-1})(\Delta G° + \lambda)^2/\lambda \quad (1)$$

where R is the edge-to-edge distance between donor and acceptor, and λ is the reorganization energy. For WT RC, a $t_{1/2}$ of 190 ns permits to obtain the value of λ: 0.61 eV. With this value of λ, we can now calculate the $t_{1/2}$ for ET from heme3 to P^+ in the mutant RC: we get $t_{1/2} = 89$ ns, whereas the measured value is 105 ns. The 105 ns phase is followed by slower phases. A phase with $t_{1/2} = 856$ ns is comparable to the F phase reported for the WT RC and which has not been interpreted otherwise than by assuming a hypothetical heterogeneity of conformation. The phase with $t_{1/2} = 11.7$ μs is presumably due to formation of ^3P [triplet state of P (*12*)].

At 350 mV, the very fast sub-microsecond kinetic term which was predominant at 157 mV disappeared, and instead a major phase with a $t_{1/2} = \sim 2$ μs arose. This phase is interpreted as being caused by the ET from heme2 via the low-potential heme, heme4, to heme3 and finally to the special pair, involving a thermodynamically unfavorable uphill step with the participation of heme4 (see later). A large part of P^+ recovers very slowly ($t_{1/2}$ above 10 ms) in RCs where all hemes of the tetraheme cyt are presumably oxidized. A good estimate of the decay half-time is 69 ms (slow phase in Table 2), which is presumably due to the back-reaction between P^+ and Q_B^-. We will now focus on the microsecond phases of the P^+ reduction.

At 350 mV, where the low-potential hemes are fully oxidized and more than 90% of heme3 in the mutant RC is also oxidized, the major fast phase has a $t_{1/2}$ of 2.2 μs. We thus assume that the source of electrons in the reaction is heme2. With WT RCs, under similar conditions, only heme3

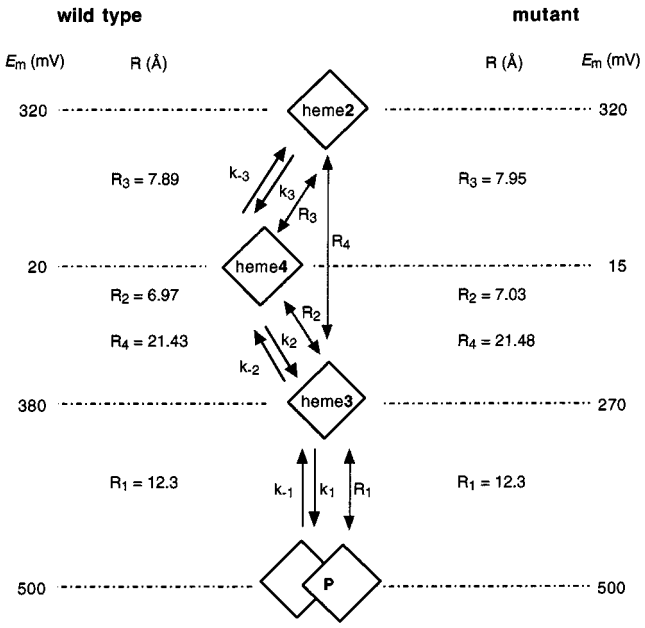

FIGURE 8: Scheme of redox centers involved in ET from heme2 to P^+ in *Rps. viridis* RC. Edge-to-edge distances (R) were measured from the X-ray structures. E_m = directly measured midpoint potentials. The rates (k_i) are those taken into consideration for the quantitative analysis (see Table 3).

is reduced and P^+ is rereduced with a $t_{1/2} = 230$ ns. A direct ET from heme2 to P^+ is practically excluded because the edge-to-edge distance is over 30 Å. Two paths can be envisioned: from heme2 directly to heme3 and then to P^+ (path 1) or a more complex path from heme2 to heme4, and then to heme3 and finally to P^+ (path 2 or uphill path, because its first step has a negative driving force). Figure 8 includes the parameters relevant for a discussion of these steps. We shall use the empirical formula of Moser and Dutton (*43*) in eq 1 in order to get a first approximation for the rate of ET of exergonic reactions. λ will arbitrarily be taken as 0.7 eV. For endergonic reactions, we first calculate the rate of the inverse exergonic reaction and then use the Boltzmann equilibrium to obtain the rate of the endergonic reaction [as suggested by Moser and Dutton (*43*)]. $\Delta G°$ is derived from the redox midpoint potentials corrected from electrostatic interactions, as proposed by Gunner and Honig (*17*). We assume identical interactions in the mutant and in the WT: 77 meV between heme3 and heme4, 14 meV between heme3 and heme2; we assume a value of 60 meV between heme4 and heme2 because these hemes are slightly more distant than heme4 and heme3. For the direct ET from heme2 to heme3, we thus calculate a $t_{1/2}$ of 0.31 s in the WT and much more in the mutant because the reaction is endergonic. We conclude that path 1 cannot account for the experimental data. For the uphill path (path 2), the results are given in Table 3, each time for forward and inverse reactions. The following features appear from Table 3.

(1) The calculated k_1 is smaller than the measured one, both in the WT and in the mutant. As discussed earlier, a better fit is obtained with $\lambda = 0.61$ eV instead of 0.70 eV.

(2) For the k_3, there is a good agreement between the calculated rates and those measured. In the WT, the half-time of 1.7 μs has been directly measured [ref *12*; other values in the literatures are very similar (*14*, *18*, *26*)]. In the mutant, we assume that in path 2 ET from heme2 to heme4

Table 3: Measured and Calculated Rates of ET in the WT and Mutant RC[a]

	k_1 ($t_{1/2}$)	k_{-1}	k_2	k_{-2}	k_3 ($t_{1/2}$)	k_{-3}
WT calcd	1.35×10^6 (515 ns)	1.2×10^4	12.9×10^9	10.2×10^4	2.95×10^5 (2.35 μs)	1.8×10^9
WT measured	3.0×10^6 (230 ns)				4.1×10^5 (1.7 μs)	
mutant calcd	4.4×10^6 (159 ns)	5.4×10^2	4.9×10^9	2.4×10^6	2.3×10^5 (3.0 μs)	1.7×10^9
mutant measured	6.6×10^6 (105 ns)				3.2×10^5 (2.2 μs)	

[a] The rates are defined in Figure 8 and the method of calculation is described in the Discussion. k (s^{-1}). It is assumed that only one high-potential heme is reduced. For the mutant, k_1 and k_{-1} are given for conditions where both high-potential hemes are reduced, which are those when k_1 can be measured. For the calculation of the uphill path in the mutant, with only heme2 reduced, $k_1 = 3.8 \times 10^6$ s^{-1} and $k_{-1} = 813$ s^{-1}. For WT RC, experimental data are from ref 12.

is the rate-limiting step in the reduction of P^+ after a flash under conditions where only heme2 is reduced. Calculated rates (Table 3) are in good agreement with that prediction. The reaction would be simple and nearly irreversible if all forward rates were much larger than backward rates. This is the case only in a rough approximation: k_1 (4.4×10^6 s^{-1}) is not much larger than k_{-2} (2.4×10^6 s^{-1}), and k_2 (4.9×10^9 s^{-1}) is not much larger than k_{-3} (1.7×10^9 s^{-1}). So, within our approximate treatment, the reduction of P^+ should include a rapid phase ($\sim$2 μs) followed by a slower nonexponential decay, but on the same time scale (0−10 μs). This may be the reason for the second phase which is observed, with a $t_{1/2}$ of 3.85 μs. Altogether, the comparison of the data with the quantitative estimate fully supports the proposal that ET from heme2 to P^+ is rate limited by uphill transfer from heme2 to heme4.

Our interpretation of the $\sim$2 μs phase makes it fully dependent on a Boltzmann equilibrium. Its activation energy can thus be calculated from the E_m of heme2 and heme4, after correction from the appropriate interaction energy calculated by Gunner and Honig (*17*), since kinetic measurements were all done under conditions when heme3 has been oxidized by rapid ET to P^+. We get 237 meV for the WT and 228 meV for the mutant. For the WT RC, the activation energy is 216 meV, as reported by Ortega and Mathis (*12*) from the measurement of ET from heme2 to heme3; for the mutant, we found 236 meV (Figure 7). The agreement is rather good in view of the experimental uncertainties and of the assumptions which had to be made. We conclude that the temperature effect on the kinetics is also in support of the mechanism proposed.

Our calculations were made with the assumption that the reorganization energy λ is 0.7 eV for each step and that is not modified by the mutation. A slightly lower value has been found by application of the empirical formula (eq 1) to ET from heme2 to P^+ in WT RC. That value is compatible with the value of 0.96 eV obtained for ET from cyt c_2 to P^+ in *Rhodobacter* (*Rb.*) *sphaeroides* RC (*44*), considering that the redox partners are better screened from the solvent in *Rps. viridis* than in *Rb. sphaeroides* where cyt c_2 is not bound permanently to the RC. In recent calculations, Moser et al. (*45*) accepted a uniform value of 1.0 eV for interheme ET in *Rps. viridis*. In any case, it should be recognized that (i) λ is not known; (ii) replacing $\lambda = 0.7$ eV by 1.0 eV has not a large effect on calculated rates; (iii) the major finding of this work, that downhill (in WT) and uphill (in the mutant) ET from heme2 to heme3 has about the same rate, leads to conclusions that do not depend on the precise value of λ.

It is generally assumed that efficient ET in biological systems should follow a regular trend from low-potential centers to high-potential ones, "downhill" in terms of free energy. That situation clearly occurs at the acceptor side of photosynthetic RCs. There are several instances, however, where ET against the redox potential gradient may take place, although the experimental arguments are not fully convincing: in multiheme cyt *c* (*46*), in hydrogenase (*47*), in nitrate reductase (*48*), or in respiratory ET chains (*49*). In the latter paper, it was suggested that uphill steps constitute possible sites for regulation.

The tetraheme cyt of *Rps. viridis* is a good system for checking the idea of uphill ET, since the reaction kinetics can be studied following a flash of light, the structure is known, and site-directed mutagenesis is available now. The source of electrons is soluble cyt c_2. In a recent paper (*21*), new kinetic data were presented, and the hypothesis fully discussed of a primary very uphill step from cyt c_2 ($E_m = +285$ mV) to heme1 ($E_m = -60$ mV). This hypothesis had already been advocated by Knaff et al. (*19*) and by Osyczka et al. (*20*).

Shopes et al. (*26*) already proposed that heme2 gets oxidized "by equilibrium with low-potential hemes", that is by an uphill reaction. Although it was not based on any structural data, their proposal is quite close to our proposal. Rappaport et al. (*14*) envisioned a direct ET from heme1 to heme4 on one hand and from heme2 to heme3 on the other hand. They find nearly the same $t_{1/2}$ for both reactions: 2.6 and 2.4 μs, respectively. We propose that this same $t_{1/2}$ is not due to coincidence, but that electrons go from heme1 to heme2 in less than 1 ns (*21*), then to heme4 in an uphill rate-limiting step with a $t_{1/2} \approx 2$ μs, then very fast to heme3, and then to P^+ in 100−200 ns. The identical $t_{1/2}$ values for oxidation of heme1 and for oxidation of heme2 are thus due to the same rate-limiting step. In this work, we provide two new arguments for the model describing ET within the tetraheme cyt: inversion of the $\Delta G°$ value by mutation does not change the $\sim$2 μs kinetics, and the reaction has the predicted activation energy.

ACKNOWLEDGMENT

We thank Dr. Dieter Oesterhelt for providing the *Rps. viridis pufC* deletion strain, Dr. Guenther Fritzsch for the setup of the microscope-photometer for redox titration on crystals and the EMBL outstation at DESY, Hamburg, for providing the beamline. We also thank Dr. Roy Lancaster for providing RC coordinates and parameters for structure refinement, and Drs. P. Bertrand, P. L. Dutton, and C. Moser for their suggestions concerning the kinetic data analysis. We thank Drs. Daniel Ungàr and Laura Baciou for critically reading the manuscript.

REFERENCES

1. Nitschke, W., and Dracheva, S. M. (1995) in *Anoxygenic Photosynthetic Bacteria* (Blankenship, R. E., Madigan, M. T., and Bauer, C. E., Eds.) pp 775−805, Kluwer Academic Publishers, Dordrecht, The Netherlands.
2. Arlt, T., Schmidt, S., Kaiser, W., Lauterwasser, C., Meyer, M., Scheer, H., and Zinth, W. (1993) *Proc. Natl. Acad. Sci. U.S.A. 90*, 11757−11761.
3. Kirmaier, C., and Holten, D. (1993) in *The Photosynthetic Reaction Center*, Vol. II (Deisenhofer, J., and Norris, J., Eds.) pp 49−70, Academic Press, San Diego.
4. Garcia, D., Richaud, P., and Verméglio, A. (1993) *Biochim. Biophys. Acta 1144*, 295−301.
5. Knaff, D. B. (1993) *Photosynth. Res. 35*, 117−133.
6. Meyer, T. E., and Donohue, T. J. (1995) in *Anoxygenic Photosynthetic Bacteria* (Blankenship, R. E., Madigan, M. T., and Bauer, C. E., Eds.) pp 725−745, Kluwer Academic Publishers, Dordrecht, The Netherlands.
7. Meyer, T. E., Bartsch, R. G., Cusanovich, M. A., and Tollin, G. (1993) *Biochemistry 32*, 4719−4726.
8. Dracheva, S. M., Drachev, L. A., Konstantinov, A. A., Semenov, A. Y., Skulachev, V. P., Arutjunjan, A. M., Shuvalov, V. A., and Zaberezhnaya, S. M. (1988) *Eur. J. Biochem. 171*, 253−264.
9. Fritzsch, G., Buchanan, S., and Michel, H. (1989) *Biochim. Biophys. Acta 977*, 157−162.
10. Verméglio, A., Richaud, P., and Breton, J. (1989) *FEBS Lett. 243*, 259−263.
11. Ortega, J. M., and Mathis, P. (1992) *FEBS Lett. 301*, 45−48.
12. Ortega, J. M., and Mathis, P. (1993) *Biochemistry 32*, 1141−1151.
13. Dohse, B., Mathis, P., Wachtveitl, J., Laussermair, E., Iwata, S., Michel, H., and Oesterhelt, D. (1995) *Biochemistry 34*, 11335−11343.
14. Rappaport, F., Béal, D., Verméglio, A., and Joliot, P. (1998) *Photosynth. Res. 55*, 317−323.
15. Deisenhofer, J., and Michel, H. (1989) *EMBO J. 8*, 2149−2170.
16. Deisenhofer, J., Epp, O., Sinning, I., and Michel, H. (1995) *J. Mol. Biol. 246*, 429−457.
17. Gunner, M. R., and Honig, B. (1991) *Proc. Natl. Acad. Sci. U.S.A. 88*, 9151−9155.
18. Dracheva, S. M., Drachev, L. A., Zaberezhnaya, S. M., Konstantinov, A. A., Semenov, A. Y., and Skulachev, V. P. (1986) *FEBS Lett. 205*, 41−46.
19. Knaff, D. B., Willie, A., Long, J. E., Kriauciunas, A., Durham, B., and Millett, F. (1991) *Biochemistry 30*, 1303−1310.
20. Osyczka, A., Nagashima, K. V. P., Sogabe, S., Miki, K., Yoshida, M., Shimada, K., and Matsuura, K. (1998) *Biochemistry 37*, 11732−11744.
21. Ortega, J. M., Drepper, F., and Mathis, P. (1999) *Photosynth. Res. 59*, 147−157.
22. Bixon, M., and Jortner, J. (1989) *Photosynth. Res. 22*, 29−37.
23. Nabedryk, E., Berthomieu, C., Verméglio, A., and Breton, J. (1991) *FEBS Lett. 293*, 53−58.
24. Nitschke, W., and Rutherford, A. W. (1989) *Biochemistry 28*, 3161−3168.
25. Shinkarev, V. P., Drachev, A. L., and Dracheva, S. M. (1990) *FEBS Lett. 261*, 11−13.
26. Shopes, R. J., Levine, L. M. A., Holten, D., and Wraight, C. A. (1987) *Photosynth. Res. 12*, 165−180.
27. Laussermair, E., and Oesterhelt, D. (1992) *EMBO J. 11*, 777−783.
28. Lang, F. S., and Oesterhelt, D. (1989) *J. Bacteriol. 171*, 2827−2834.
29. Claus, D., and Schaab-Engels, C., Eds. (1977) *German collection of microorganisms, Catalogue of strains*, 2nd ed., pp 279−280, Deutsche Sammlung von Mikroorganismen und Zellkulturen GmbH, Braunschweig, Germany.
30. Devereux, J., Haeberli, P., and Smithies, O. (1984) *Nucleic Acids Res. 12*, 387−395.
31. Kunkel, T. A., Roberts, J. D., and Zakour, R. A. (1987) *Methods Enzymol. 154*, 367−382.
32. Porath, J., Carlsson, J., Olsson, I., and Belfrage, G. (1975) *Nature 258*, 598−599.
33. Goldsmith, J. O., and Boxer, S. G. (1996) *Biochim. Biophys. Acta. 1276*, 171−175.
34. Clayton, R. K., and Clayton, B. J. (1978) *Biochim. Biophys. Acta 501*, 478−487.
35. Michel, H. (1982) *J. Mol. Biol. 158*, 567−572.
36. Otwinowski, Z. (1993) in *Proceedings of the CCP4 Study Weekend, 29−30 Jan, 1993, Data Collection and Processing* (Sawyer, L., Isaacs, N., and Bailey, S., Eds.) pp 56−62, SERC Daresbury Laboratory, England.
37. Lancaster, C. R. D., and Michel, H. (1997) *Structure 5*, 1339−1359.
38. Bruenger, A. T. (1991) *Annu. Rev. Phys. Chem. 42*, 197−223.
39. Jones, T. A., Zou, J. Y., Cowan, S. W., and Kjeldgaard, M. (1991) *Acta Crystallogr., Sect. A 47*, 110−119.
40. Wiessner, C., Dunger, I., and Michel, H. (1990) *J. Bacteriol. 172*, 2877−2887.
41. Weyer, K. A., Lottspeich, F., Gruenberg, H., Lang, F., Oesterhelt, D., and Michel, H. (1987) *EMBO J. 6*, 2197−2202.
42. Mathews, F. S. (1985) *Prog. Biophys. Mol. Biol. 45*, 1−56.
43. Moser, C. C., and Dutton, P. L. (1992) *Biochim. Biophys. Acta 1101*, 171−176.
44. Venturoli, G., Drepper, F., Williams J. C., Allen, J. P., Lin, X., and Mathis, P. (1998) *Biophys. J. 74*, 3226−3240.
45. Moser, C. C., Keske, J. M., Warncke, K., Farid, R. S., and Dutton, P. L. (1998) Nature *355*, 796−802
46. Bertrand, P., Asso, M., Mbarki, O., Camensuli, P., More, C., and Guigliarelli, B. (1994) *Biochimie 76*, 524−536.
47. Volbeda, A., Charon, M., Piras, C., Hatchikian, E. C., Frey, M., and Fontecilla-Camps, J. C. (1995) *Nature 373*, 580−587.
48. Guigliarelli, B., Magalon, A., Asso, M., Bertrand, P., Frixon, C., Giordano, G., and Blasco, F. (1996) *Biochemistry 35*, 4828−4836.
49. Dutton, P. L., Chen, X., Page, C. C., Huang, S., Ohnishi, T., and Moser, C. C. (1998) in *Biological Electron-Transfer Chains* (Canters, G. W., and Vijgenboom, E., Eds.) pp 3−8, Kluwer Academic Publishers, Dordrecht, The Netherlands.
50. Luzzati, P. V. (1952) *Acta Crystallgr. 5*, 802−810.

BI992443P